Global and Planetary Change 165 (2018) 100–113

Contents lists available at ScienceDirect

Global and Planetary Change

journal homepage: www.elsevier.com/locate/gloplacha

Research article

A probabilistic method for streamflow projection and associated uncertainty analysis in a data sparse alpine region

Weiwei Ren[a,c], Tao Yang[a,b,*], Pengfei Shi[b], Chong-yu Xu[b,d], Ke Zhang[b,e], Xudong Zhou[b,g], Quanxi Shao[f], Philippe Ciais[g]

[a] State Key Laboratory of Desert and Oasis Ecology, Xinjiang Institute of Ecology and Geography, Chinese Academy of Sciences, Urumqi 830011, China
[b] State Key Laboratory of Hydrology-Water Resources and Hydraulic Engineering, Center for Global Change and Water Cycle, Hohai University, Nanjing 210098, China
[c] University of Chinese Academy of Sciences, Beijing 100049, China
[d] Department of Geosciences, University of Oslo, P.O. Box 1047, Blindern, 0316 Oslo, Norway
[e] Cooperative Institute for Mesoscale Meteorological Studies, University of Oklahoma, 120 David L. Boren Blvd., Norman, OK 73072, USA
[f] CSIRO Digital Productivity Flagship, Leeuwin Centre, 65 Brockway Road, Floreat, WA 6014, Australia
[g] Laboratorie des Sciences du Climat et de l'Environnement, Commissariat a L'Energie Atomique, 91191 Gif sur Yvette, France

ARTICLE INFO

Editor: Sierd Cloetingh

Keywords:
Climate change
Streamflow projection
Bayesian neural networks
Flexible model structures
Active indicator function
Least-Square Support Vector Machine
Uncertainty estimates
Data sparse alpine region

ABSTRACT

Climate change imposes profound influence on regional hydrological cycle and water security in many alpine regions worldwide. Investigating regional climate impacts using watershed scale hydrological models requires a large number of input data such as topography, meteorological and hydrological data. However, data scarcity in alpine regions seriously restricts evaluation of climate change impacts on water cycle using conventional approaches based on global or regional climate models, statistical downscaling methods and hydrological models. Therefore, this study is dedicated to development of a probabilistic model to replace the conventional approaches for streamflow projection. The probabilistic model was built upon an advanced Bayesian Neural Network (BNN) approach directly fed by the large-scale climate predictor variables and tested in a typical data sparse alpine region, the Kaidu River basin in Central Asia. Results show that BNN model performs better than the general methods across a number of statistical measures. The BNN method with flexible model structures by active indicator functions, which reduce the dependence on the initial specification for the input variables and the number of hidden units, can work well in a data limited region. Moreover, it can provide more reliable streamflow projections with a robust generalization ability. Forced by the latest bias-corrected GCM scenarios, streamflow projections for the 21st century under three RCP emission pathways were constructed and analyzed. Briefly, the proposed probabilistic projection approach could improve runoff predictive ability over conventional methods and provide better support to water resources planning and management under data limited conditions as well as enable a facilitated climate change impact analysis on runoff and water resources in alpine regions worldwide.

1. Introduction

The arid inland area of Xinjiang is located in Central Asia, far from seas and surrounded by high mountains (Kunlun, Tien and Altai), and hydrological and ecological processes there are highly sensitive to climate change (Shi et al., 2016). The streamflow mainly comes from alpine rainfall, and snow and glacier melting, which provide basic water sources to support people's livelihood and socio-economic development (Wang et al., 2013; Chen et al., 2013). Recently, global warming has led to glacier and snow cover retreat (Yang et al., 2014) and precipitation pattern change in this region (Wang et al., 2016; Shi et al., 2017), affecting runoff regime of rivers and water availability (Zhang et al., 2009a; Yang et al., 2015).

Public interest and awareness of the importance of change in hydrological processes have increased sharply in recent years (Xu et al., 2011; Shen et al., 2013). IPCC5 (2013) pointed out that global air temperature has increased by 0.06 °C/decade during the period 1880–2012. The average annual temperature in the Xinjiang arid area is rising even more significantly, at the rate of 0.32 °C/decade in the recent 50 years (Shen et al., 2013; Yang et al., 2012). Climate change is projected to continue in the future (IPCC5, 2013), which will impose profound influence on regional water balance and socio-economic

* Corresponding author at: State Key Laboratory of Hydrology-Water Resources and Hydraulic Engineering, Center for Global Change and Water Cycle, Hohai University, Nanjing 210098, China.
E-mail address: tao.yang@hhu.edu.cn (T. Yang).

https://doi.org/10.1016/j.gloplacha.2018.03.011
Received 14 May 2017; Received in revised form 11 March 2018; Accepted 19 March 2018
Available online 30 March 2018

development in this region. Therefore, robust projections of streamflow under climate change are of vital importance to understand consequences of climate change in this region.

In general, scenarios from Global Circulation Models (GCMs) or Regional Climate Models, statistical downscaling methods and hydrological models are common tools to study the impacts of climate change on hydrological processes. However, the current conventional approaches based on these tools (Lutz et al., 2014; Dickerson-Lange and Mitchell, 2014; Yang et al., 2017a) require a large number of input data on topography, land-use, soil type, as well as meteorological and hydrological data. However, many alpine regions across the world have limited hydrological and meteorological observation networks. Without a solid support of sufficient input data, complex algorithms could introduce considerable uncertainties into the simulation results, consequently leading to a high risk for decision making on water resources and eco-environmental management.

This calls for efforts to directly simulate and project river runoff using GCMs or reanalysis data based on statistical downscaling approach. It is a direct streamflow downscaling without traditional hydrological modeling. For example, Cannon and Whitfield (2002) built a direct model to investigate streamflow changes using an ensemble of neural networks forced by NCEP/NCAR reanalysis data in British Columbia, Canada. The results showed that the model was capable of capturing the non-linear interactive relationships between climate variables and runoff. Ghosh and Mujumdar (2008) constructed a direct streamflow model at the river basin scale to apply for monsoon period, and projected the future streamflow using IPCC4-GCM simulated climatic variables. Tisseuil et al. (2010) employed four models for downscaling NCEP/NCAR reanalysis and GCM outputs to daily and fortnightly streamflows at 51 stations in France. The results revealed that fortnightly downscaling model outperforms daily downscaling model. Sachindra et al. (2013) developed a direct model projecting monthly streamflow from the monthly GCM outputs. Okkan and Inan (2015) predicted the monthly inflows of Kemer Dam in Turkey using direct streamflow downscaling method. Presently, the studies of streamflow downscaling at daily scale mainly focus on mechanism research, for example, Tisseuil et al. (2010) compared the performances of different models under different hydrological conditions and explored relationship between atmospheric factors and streamflow variability. However, with respect to future hydrological projections or studying climate change impacts on streamflow, the researchers tend to use monthly streamflow downscaling. For instance, Okkan and Inan (2015) predicted the streamflow of Kemer Dam at monthly scale, and Tisseuil et al. (2010) predicted median flow based on the regional bimonthly downscaling approach. This is likely due to streamflows downscaling on daily scale has larger uncertainties than that of monthly since GCMs (Bates et al., 1998) and reanalysis data (Wang and Zeng, 2012) perform well in simulating climatic variables at larger time scales but poorly at the smaller time scales.

Direct streamflow downscaling is one of the few ways to project streamflows into future, which has two obvious advantages over the conventional modeling framework. On the one hand, statistical downscaling involves low computational costs and can be implemented without detailed knowledge of the physical processes of the hydrologic cycle (Sachindra et al., 2013). On the other hand, direct streamflow downscaling is not subject to uncertainties originating from downscaling multiple variables (e.g., precipitation, temperature) and complex hydrologic processes. However, the direct downscaling approach generally do not take into account the physical factors affecting the streamflow variability such as the land use and soil type, assuming deterministically that those factors do change with time (Tisseuil et al., 2010). Consequently, this approach can't reflect the impacts of land use change on streamflow in the areas where severely affected by human activities, such as diversion irrigation and reservoir regulation. Thus, Sachindra et al. (2015) deemed this approach can only be used for simulation of unregulated flows in a catchment.

Recently, various statistical algorithms (e.g., Artificial Neural Network, ANN (Gao et al., 2010; Wang et al., 2012), Canonical Correlation Analysis, CCA (Landman et al., 2001), and Relevance Vector Machine, RVM (Okkan et al., 2014)) have been increasingly used to solve various hydrological problems. Due to high efficiency in characterizing non-linear dependencies between the inputs and outputs without considering fundamental physical processes, the ANN technique has been applied to simulate and project streamflow (Zeng et al., 2012). However, one major limitation of ANN is that the neural networks are trained by a maximal likelihood function of parameters, and hence the uncertainty of the predicted variables has seldom been quantified (Khan and Coulibaly, 2006; Zhang et al., 2009b). Facing the huge uncertainties arising from data scarcity, the aforementioned deterministic methods (RVM, CCA, ANN) generally fail to provide both efficient simulation and uncertainty estimation for streamflow, especially in data-scarce regions.

Thus, a new approach that enables a direct runoff projection and associated uncertainty estimation is urgently needed. The Bayesian Neural Networks (BNN) widely used in agriculture, medical science and engineering in the last decades (Beam et al., 2014; Niu et al., 2012; Zhou et al., 2017), provides a probabilistic approach to simulate and estimate uncertainties. For example, Zhang et al. (2009b) proposed a BNN-based model for streamflow simulation, and successfully estimated uncertainty using BNNs. The results showed that the BNN probabilistic model outperformed the traditional ANN deterministic model in terms of prediction accuracy and confidence intervals estimation.

Considering the convenience of directly projecting streamflow and the advantages of BNN, this method was used to evaluate the impacts of climate change (Khan and Coulibaly, 2010). However, there are still some flaws in this method (i.e. large uncertainties existing in the inputs), and the fixed structure of a traditional BNN model has dependence on input variables. Therefore, a pertinent modeling framework for streamflow projection using GCMs effectively conquering data scarcity problem is limited so far. Consequently, development of a framework to effectively project streamflow in conditions of data scarcity, together with uncertainty estimation and assessment of climate impacts is needed. Toward this end, this work seeks to: (1) build a consolidated streamflow projection model by means of BNN with flexible model structures via active indicator functions; (2) inter-compare the skills in reproducing streamflow by the new and traditional approaches (using BNN, LSSVM and SWAT model); and (3) construct robust projections of streamflow by the BNN model using a series of the latest bias-corrected GCMs, and estimate uncertainty in a typical data sparse alpine region.

2. Study area and data

2.1. Study area

The Kaidu River (42°14′-43°21′ N, 82°58′-86°05′ E) is one of the main tributaries of the Tarim River in Central Asia. It originates from the central Tien Shan Mountains in the northwest China (Fig. 1). The river starts from Hargat and Jacsta Valleys in Sarming Mountain with a maximum altitude of 4796 m (the middle Tien Shan Mountains) and ends at Bosten Lake located in Bohu County of Xinjiang province. The drainage area above the Dashankou hydrological station is 18,827 km^2, with an average elevation of 3100 m (Tao et al., 2007), and has one meteorological station shown in Fig. 1. About 473.97 km^2 of the basin area is covered by glaciers and snow packs, including Erwengen, Yilianhabierduo, Haerlek and Nalati Mountains, where elevation is between 4000 and 4500 m. The streamflow is mainly recharged by snowmelt during spring and glacier-melt and rainfall during summer.

The basin has a typical alpine climate with an average annual temperature of −4.16 °C. The annual average precipitation is 273 mm, whereas potential evaporation is 1157 mm. The annual precipitation

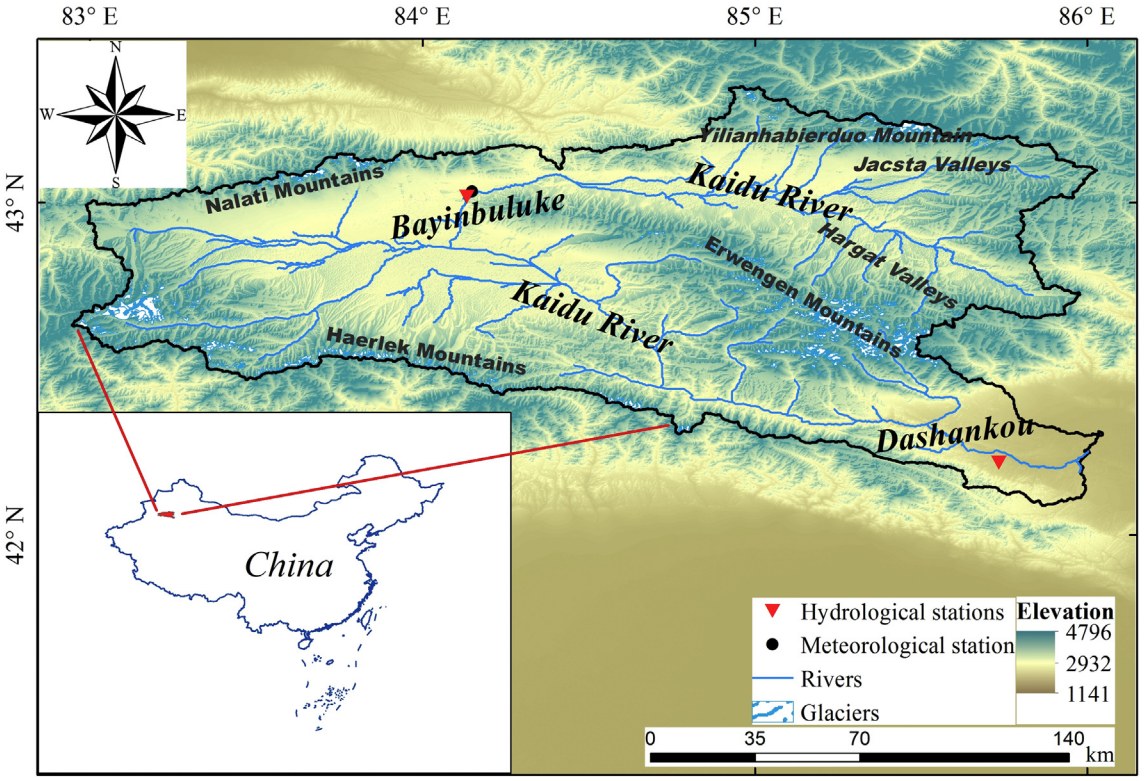

Fig. 1. Map of Kaidu River Basin.

varies along elevation: higher precipitation (200–500 mm) in mountainous areas, and lower (50–80 mm) in valleys. Precipitation also changes with seasons. More than 80% of precipitation falls between May and September. On average, there are 139 snow-cover days in the basin, and the largest average annual snow depth is 12 cm (Xu et al., 2008). 70% of runoff occurs between May and October. The average runoff is 78.4 million m^3/day in spring, 168.5 million m^3/day in summer, and 81.2 million m^3/day in autumn.

2.2. Data

The observed unregulated monthly streamflow data at the Dashankou hydrological station from 1979 to 2014 were collected from the Xinjiang Hydrological Bureau. In downscaling studies, predictors derived from the large-scale circulation variables (Wetterhall et al., 2005; Anandhi et al., 2008) should be: (*a*) reliably simulated and available from GCM outputs or reanalysis data, and (*b*) strongly correlated with the surface variables of interest. In this study, the streamflow of Kaidu River in temperate continental climate characteristics was mainly affected by precipitation and temperature (Zhuang et al., 2018). The study of Liu et al. (2011) showed that the precipitation in these regions is mainly influenced by specific humidity, v-component of wind. Sea-level pressure, u-component of wind are the secondary climatic factors for precipitation. And precipitation in Tien Shan is mainly controlled by westerly water vapor transport (Dai et al., 2007; Qian and Qin, 2008). While, temperature is generally controlled by specific humidity, geopotential and wind. Besides, the 500 hPa and 850 hPa circulation variables (i.e., geopotential and wind component) are usually used as predictors for downscaling GCM outputs to temperature, precipitation and streamflow (Yang et al., 2017b; Wang et al., 2012; Tisseuil et al., 2010; Sachindra et al., 2015; Okkan and Inan, 2015). Finally, 15 predictors (Table 1) were selected as potential predictors. These predictor variables were compiled from the Japanese 55-year Reanalysis (JRA55) project of the Japan Meteorological Agency (JMA) (http://jra.kishou.go.jp/JRA-55/index_en.html) for the period from 1958 onward, with a spatial resolution of 1.25° × 1.25°. In this project, a state-of-the-art four-dimensional variational data assimilation (4D-Var) system with Variational Bias Correction (VarBC) was used in order to eliminate some deficiencies in the Japanese 25-year Reanalysis data (Ebita et al., 2011). Usually, NCEP/NCAR Reanalysis Data is used to offer atmospheric predictors for climate change studies, but it has some human processing errors and system errors (Kanamitsu et al., 2002). Thus the NCEP/DOE Reanalysis II (NCEP-II) was run to address some of these problems (Kanamitsu et al., 2002) and regarded as an updated version of NCEP/NCAR. To make sure whether JRA55 or NCEP-II is more suitable for this study, these datasets were obtained for the region spanning 40.0°–43.75° N and 82.50°–87.50° E at monthly scale from 1979 to 2014 and compared. Finally, the JRA55 data was selected for this study based on the preferable performance over the NCEP-II (Table S1).

In order to decrease the uncertainty of single model, five bias-corrected GCMs (i.e., HadGEM2-ES, MIROC-ESM-CHEM, NorESM1-M, IPSL-CM5A-LR and GFDL-ESM2M) participating in the fifth phase of the Climate Model Inter-comparison Project (CMIP5) (Taylor et al., 2012) were used as climate forcing. These five bias-corrected GCMs provided by the Inter-Sectoral Impact Model Inter-comparison Project (ISI-MIP) (https://esg.pik-potsdam.de/search/isimip/) were corrected by the trend-preserving bias correction method (Hempel et al., 2013). This method used the WATCH Forcing Data (Weedon et al., 2011) including ERA-40 data (i.e., the 40-yr reanalysis of the European Centre for Medium Range Weather Forecasts), CRU data (i.e., the Climate Research Unit TS2.1 dataset) and GPCC data (i.e., the Global Precipitation Climatology Centre full dataset version 4) for the period from 1 January 1960 to 31 December 1999 (the reference period) as an observation-based reference dataset. The average trends of different variables between the observations and the GCMs in the reference period were calculated by different methods. Following this, the trend was used as a constant offset or multiplicative correction factor to correct the variables of GCMs (Hempel et al., 2013). The projections by these five models under three RCP scenarios - RCP2.6, RCP4.5 and RCP8.5 were

Table 1
Candidate predictor variables.

	Monthly variable	Code	Monthly variable	Code
Variables	Mean temperature at 2 m	tmp	Near surface specific humidity	huss
	Mean sea level pressure	mslp	u-component of wind at 10 m	uas
	500 hpa geopotential height	hgt500	u-component of wind at 500pha height	ua500
	850 hpa geopotential height	hgt850	u-component of wind at 850pha height	ua850
	Near surface relative humidity	hurs	v-component of wind at 10 m	vas
	Relative humidity at 500pha height	hur500	v-component of wind at 500pha height	va500
	Relative humidity at 850pha height	hur850	v-component of wind at 850pha height	va850
	Monthly total precipitation	pr		

applied. The datasets were uniformly aggregated into 1.25° × 1.25° grid cells at monthly scale to match the resolution of the JRA-55 reanalysis data.

The daily meteorological data from the Bayinbuluke station for the SWAT model were downloaded from the China Meteorological Data Sharing Service Network (http://cdc.cma.gov.cn/satellite). The Digital Elevation Model (DEM) with grid size of 90 m was obtained from the CGIAR Consortium for Spatial Information (CGIAR-CSI) (http://eros.usgs.gov/find-data). The digital topographic data were used to delineate watersheds into sub-basins, generate river network, and define water bodies and outlets. Soil characteristics were derived from the Harmonized World Soil Database (HWSD) of Food and Agriculture Organization of the United Nations (http://www.fao.org/soils-portal/soil-survey/soil-maps-and-databases/harmonized-world-soil-database-v12/en/), with a spatial resolution of about 1000 m. Land cover characteristics were extracted from the MERIS Glob-cover product (http://due.esrin.esa.int/globcover/). The land cover was based on the latest version of the world satellite maps in 2009 of the European Space Agency, with a spatial resolution of 300 m.

3. Methodology

In this study, a probabilistic model based on BNN with flexible model structures using active indicator functions is built to predict monthly streamflow and applied to the Kaidu River. The framework (Fig. 2) can be summarized as following: step 1: to identify the dominant impact factors from the reanalysis datasets JRA55 on streamflow based on stepwise regression approach, step 2: to build an advanced BNN model with the flexible model structures less dependent on input variables to simulate and project streamflow, step 3: to evaluate the

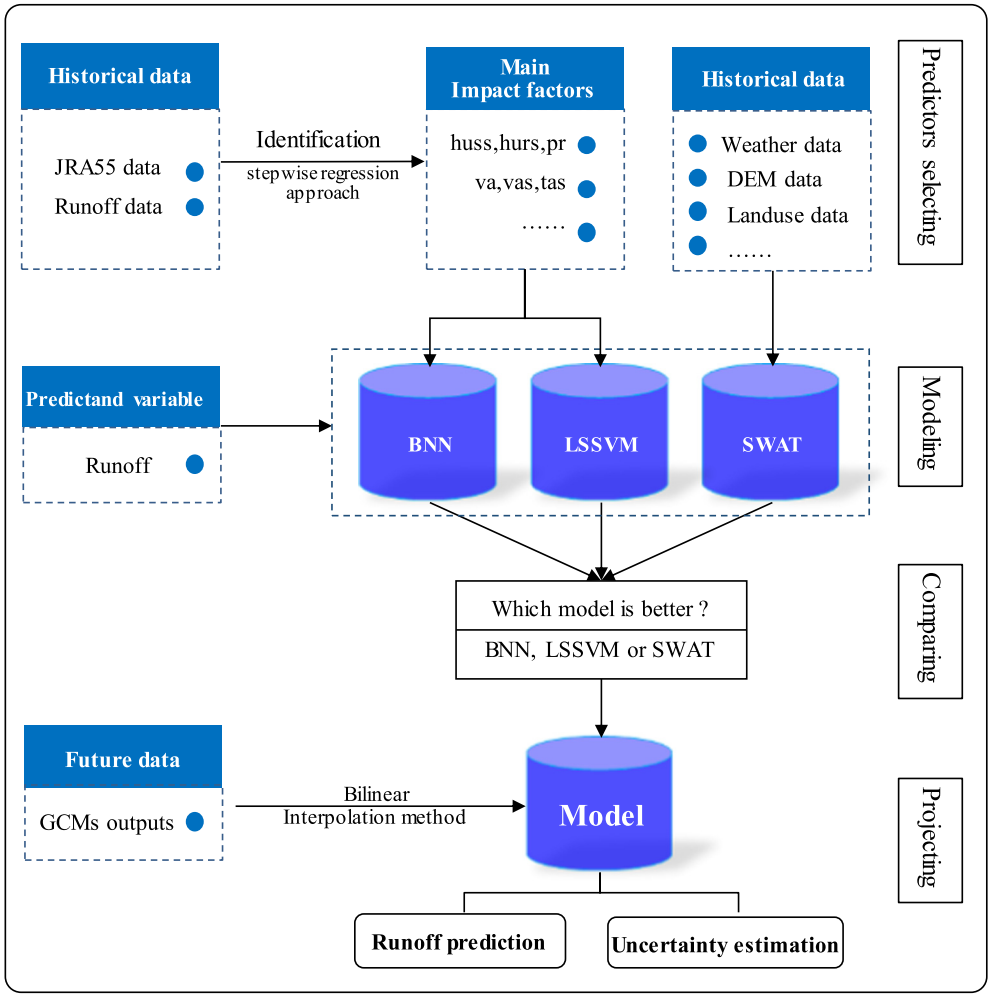

Fig. 2. Overview of model framework for Kaidu River runoff prediction.

performance of the BNN model through a comparison with the LSSVM and SWAT models, and step 4: to construct future projections of streamflow for the period 2017–2099 and analyze streamflow changes in the future and associated uncertainty in the basin under three emission scenarios in multiple time horizons.

3.1. Bayesian neural networks

The BNN is trained based on the joint posterior of the network structure and weights assigned by an Evolutionary Monte Carlo (EMC) method. There are three main reasons for the selection of the BNN model. First, the structure of BNN is variable, which is proved to be better than the fixed structure (Zhang et al., 2009b). Second, BNN is trained by the EMC method to avoid the problem of local minimum convergence, which is generally encountered in the traditional neural networks training (Liang, 2005). Third, BNN can also estimate the predictive confidence intervals which indicate the prediction quality. Basically, the BNN is a three-layer neural network with inputs units, hidden units and output unit, as shown in Fig. 3.

The BNN has a series of variable connections obtained by adding a set of indicator functions into the intrinsic structure (Liang and Kuk, 2004). The BNN model can be represented by:

$$\widehat{f}(x_t) = \alpha_0 I_{\alpha_0} + \sum_{i=1}^{p} x_{it}\alpha_i I_{\alpha_i} + \sum_{j=1}^{M} \beta_j I_{\beta_j} \psi\left(\gamma_{j_0} I_{\gamma_{j0}} + \sum_{i=1}^{p} x_{it}\gamma_{ji} I_{\gamma_{ji}}\right) \quad (1)$$

where x_t is the input data vector at time t; p is the dimension of x_t; x_{it} is the ith component of x_t; M is the number of hidden units; α_0 denotes the bias of the output unit; α_i denotes the weight on the shortcut connection from the ith input unit to the output unit; β_j denotes the weight on the connection from the jth hidden unit to the output unit; γ_{j0} denotes the bias of the jth hidden unit; γ_{ji} denotes the weight on the connection from the i th input unit to the j th hidden unit; $\psi()$ is the activation function of the hidden units. I_ζ is the active indicator function associated with the connection ζ. If $I_\zeta = 1$, then the connection is in effect; otherwise, $I_\zeta = 0$ and the connection is not effective. These indicator functions make it more flexible for BNN to control the effect of each connection. The total number of effective active indicator functions is $\Sigma_{i=0}{}^{p} I_{\alpha i} + \Sigma_{j=1}{}^{M} I_{\beta j}\delta(\Sigma_{i=0}{}^{p} I_{\gamma ji}) + \Sigma_{j=1}{}^{M}\Sigma_{i=0}{}^{p} I_{\beta j} I_{\gamma ji}$, where $\delta(z)$ is 1 if $z > 0$ and 0 otherwise. The I_ζ was initialized randomly as 1 or 0, and then was automatically adjusted by the EMC model. In this study, we set $\psi(z) = \tanh(z)$ for all examples to ensure that the output of a hidden unit is 0, if all connections to the hidden unit from input units have been eliminated. Thus, a hidden unit can be eliminated from the network without any effect on the network outputs.

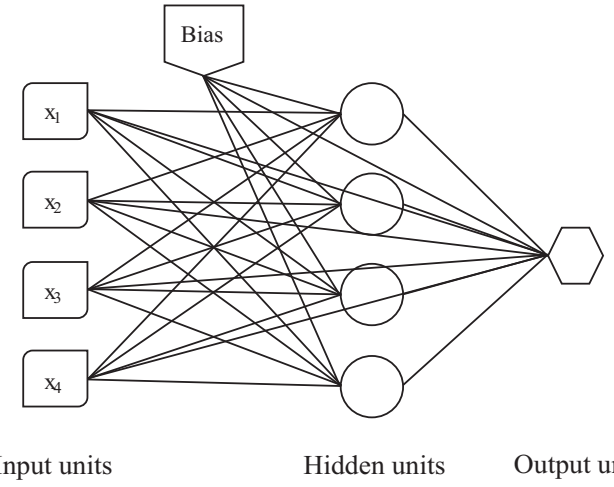

Fig. 3. A fully-connected one-hidden-layer neural network with input units, hidden units, and output unit.

In this study, Λ is used to specify the structure of the network, consisting of all active indicators in Eq. (1). Simultaneously, we let $\alpha = (\alpha_0, \alpha_1, \ldots, \alpha_p)$, $\beta = (\beta_0, \beta_1, \ldots, \beta_M)$, $\gamma_j = (\gamma_{j_0}, \gamma_{j_1}, \ldots, \gamma_{j_p})$, $\gamma = (\gamma_1, \ldots, \gamma_M)$ and $\theta = (\alpha, \beta, \gamma, \sigma^2)$, where α_Λ, β_Λ and γ_Λ denote the non-zero subsets of α, β and γ, respectively. Usually, the large weights and bias values and complex model structures are penalized. We follow Liang (2005) to assume the following priori distributions for the weights: $\alpha_i \sim N(0, \sigma_\alpha{}^2)$, for $i = 0, \ldots p$, $\beta_j \sim N(0, \sigma_\beta{}^2)$, for $j = 0, \ldots, M$, $\gamma_{ij} \sim N(0, \sigma_\gamma{}^2)$, for $j = 0, \ldots, M$ and $i = 0, \ldots p$ where $\sigma_\alpha{}^2$, $\sigma_\beta{}^2$ and $\sigma_\gamma{}^2$ are hyper-parameters that are set to Inverse Gamma distributions ($\sigma_\alpha{}^2$, $\sigma_\beta{}^2$, $\sigma_\gamma{}^2 \sim IG(v_1, v_2)$). Thus the combination of (θ, Λ) completely defines Eq. (1).

3.2. Training of the Bayesian neural networks

The combination of θ and Λ, representing the neural network's parameters and the network's structures, defines the neural network model. In the traditional deterministic training of a neural network, a single set of optimal (θ, Λ) is identified to most likely reproduce the observed target data. From the perspective of Bayesian, the essence of training the BNN is an inference problem. Therefore, constructing the posterior probability distribution of (θ, Λ) becomes the main task of the Bayesian approach. In the Bayesian training framework, the posterior probability distribution could modify the original distribution, and adjust the parameters more reasonably through a comprehensive use of priori probability distribution, sample information and model structure. Given the training data sets $D = \{(x_1, y_1), (x_2, y_2), \ldots, (x_n, y_n)\}$, the posterior distribution of the weights and model structure (θ, Λ) is defined as

$$p(\theta, \Lambda \mid D) = \frac{p(D \mid \theta, \Lambda)\pi(\theta, \Lambda)}{m(D)} \quad (2)$$

where $p(\theta, \Lambda | D)$ is the posterior probability distribution of (θ, Λ) given observed data D; $m(D)$ is the marginal distribution of D and independent on θ and Λ. In this study, $m(D) = \int p(D|\theta, \Lambda)\pi(\theta, \Lambda)d(\theta, \Lambda)$ and is the normalizing constant. $\pi(\theta, \Lambda)$ is the priori probability distribution of (θ, Λ); $p(D|\theta, \Lambda)$ is the likelihood function of (θ, Λ), which is denoted as $L(\theta, \Lambda)$. To conduct the training of the BNN, the priori probability distribution $\pi(\theta, \Lambda)$ and the likelihood function $L(\theta, \Lambda)$ need to be specified. Commonly, it is assumed that the model residuals are independent and belong to the Gaussian distribution ($\sim N(0, \sigma^2)$) to specify the likelihood function. Thus, we have the likelihood function:

$$L(\theta, \Lambda) = p(y \mid \theta, \Lambda, x) = \left\{\prod_{t=1}^{n} \frac{1}{\sqrt{2\pi\sigma^2}} \exp\left(-\frac{(y_t - f(x_t))^2}{2\sigma^2}\right)\right\} \quad (3)$$

where n is the number of observed target data, and σ^2 is referred to as a hyper-parameter which is assumed to belong to an inverse gamma (IG) distribution ($\sigma^2 \sim IG(v_3, v_4)$), with v_3 and v_4 the shape parameters and scale parameter, respectively. The basic probability density function of the inverse gamma (IG) distribution is

$$f(x) = \frac{\beta^\alpha}{\Gamma(\alpha)} x^{-\alpha-1} \exp\left(-\frac{\beta}{x}\right) \qquad (\alpha > 0, x > 0) \quad (4)$$

where α and β are the shape parameter and scale parameter, respectively. Following Liang (2005) and Zhang et al. (2009b), the priori distribution of the neural network structure Λ is set to be subject to a priori probability that is proportional to a truncated Poisson distribution.

$$p(\Lambda) = \begin{cases} \frac{1}{z}\frac{\lambda^\omega}{\omega} & \omega = 3, 4, \ldots, U \\ 0 & otherwise \end{cases} \quad (5)$$

where λ is a hyper-parameter, $U = (H + 1)(p + 1) + H$ is the number of connections of the full model in which all connections are valid (i.e. all $I_\zeta = 1$), $Z = \Sigma_{\Lambda \in \Omega}\lambda^\omega/\omega!$ and Ω is a set of all possible model structures

with $\omega = 3, 4, \ldots, U$. The minimum number of ω is set to three, which is small enough as a limiting network size. Eq. (5) gives a higher priori weight to the neural networks with simpler structure (i.e., fewer effective connections). Generally, the number of effective connections is much less than U. That is to say, in this BNN model, the input variables are selected automatically by EMC which sample from the joint posterior of the network structure (Λ) and weights. As a result of this, only parts of the input variables are used in the model.

$$
\begin{aligned}
p(\theta, \Lambda | D) = & \left\{ \prod_{i=0}^{P} \varphi \left\{ I_{a_i}, \left[\frac{1}{\sqrt{2\pi\sigma_\alpha{}^2}} \exp\left(\frac{-\alpha_i{}^2}{2\sigma_\alpha^2} \right) \right], 1 \right\} \right\} \\
& \times \left\{ \frac{\nu_2{}^{\nu_1}}{\Gamma(\nu_1)} (\sigma_\alpha{}^2)^{-\nu_1-1} \exp\left(\frac{-\nu_2}{\sigma_\alpha{}^2} \right) \right\} \\
\times & \left\{ \prod_{j=0}^{H} \varphi \left\{ I_{\beta_j} \Phi \left(\sum_{i=0}^{P} I_{\gamma_{ji}} \right), \left[\frac{1}{\sqrt{2\pi\sigma_\beta{}^2}} \exp\left(\frac{-\beta_j^2}{2\sigma_\beta^2} \right) \right], 1 \right\} \right\} \\
& \times \left\{ \frac{\nu_2{}^{\nu_1}}{\Gamma(\nu_1)} (\sigma_\beta{}^2)^{-\nu_1-1} \exp\left(\frac{-\nu_2}{\sigma_\beta{}^2} \right) \right\} \\
\times & \left\{ \prod_{j=0}^{H} \varphi \left\{ I_{\beta_j}, \prod_{i=0}^{P} I_{\gamma_{ji}} \left[\frac{1}{\sqrt{2\pi\sigma_\gamma{}^2}} \exp\left(\frac{-\gamma_{ji}{}^2}{2\sigma_\gamma^2} \right) \right], 1 \right\} \right\} \\
& \times \left\{ \frac{\nu_2{}^{\nu_1}}{\Gamma(\nu_1)} (\sigma_\gamma{}^2)^{-\nu_1-1} \exp\left(\frac{-\nu_2}{\sigma_\gamma{}^2} \right) \right\} \\
\times & \left\{ \prod_{i=1}^{n} \left[\frac{1}{\sqrt{2\pi\sigma^2}} \exp\left(-\frac{(y_t - f(x_t))^2}{2\sigma^2} \right) \right\} \times \left\{ \frac{\nu_4{}^{\nu_3}}{\Gamma(\nu_3)} (\sigma^2)^{-\nu_3-1} \exp\left(\frac{-\nu_4}{\sigma^2} \right) \right\} \right. \\
& \times \left\{ \frac{1}{Z} \frac{\lambda^\omega}{\omega} \right\}
\end{aligned}
\tag{6}
$$

Furthermore, following the Liang's (2005) assumption that the components of θ and Λ are a priori independent, and that the priori distributions of θ and Λ are independent, the posterior distribution of (θ, Λ) can be formalized by multiplying the priori distributions of θ, Λ and $L(\theta, \Lambda)$.

By integrating the predictions of the model with respect to the posterior distribution of the model (θ, Λ), the posterior predictive distribution of output y_{new} for the new input x_{new} is

$$
p(y_{new} \mid x_{new}, D) = \int p(y_{new} \mid x_{new}, \theta, \Lambda) p(\theta, \Lambda \mid D) d(\theta, \Lambda) \tag{7}
$$

The expectation of the posterior prediction distribution in Eq. (3) is

$$
\widehat{y}_{new} = E(y_{new} \mid x_{new}, D) = \int f(x_{new}, \theta, \Lambda) p(\theta, \Lambda \mid D) d(\theta, \Lambda) \tag{8}
$$

In this study, the EMC method is used for sampling the posterior probability of model structures and parameters of BNN. The EMC method was originally designed for sampling from a distribution defined in a fixed dimensional space. Afterwards, it was applied by Liang (2005) to sample from a distribution defined in the variable dimensional spaces. The EMC algorithm, developed based on the combination of parallel tempering, reversible jump MCMC (Monte Carlo methods combined with Markov chain) and the genetic algorithm, combines the strength of the genetic algorithm for parameter optimization and the capacity of MCMC for generating samples observing target distribution (Liang and Wong, 2001). It can help to avoid the local convergence commonly encountered in training. Specific mutation and crossover, exchange operators are designed for the BNN models. In EMC, the complex integrals in the marginalization are approximated via drawing samples from the joint probability distribution of (θ, Λ), and $\widehat{y}_{new}$ can be approximated using a sample of the (θ, Λ) drawn from the posterior probability distribution of (θ, Λ):

$$
\widehat{y}_{new} = \frac{1}{K} \sum_{i=1}^{K} f(x_{new}, \theta_i, \Lambda_i) \tag{9}
$$

here K denotes the accepted number of the final samples.

3.3. The Least-Square Support Vector Machine method

The Support Vector Machines (SVMs) were firstly put forward in early 1990s (Vapnik, 1995) based on the statistical learning theory for classification purposes. The SVMs have been extended successfully not only for regression but also for hydrologic applications (Kalra and Ahmad, 2012). Since the SVMs can automatically answer crucial questions when involved in the construction of a resulting network, it is often regarded as an attractive solution in the artificial intelligence type problems. However, with the increase of the amount of data, the shortcomings of high computational complexity and time-consuming become more apparent. To overcome this drawback, Suykens et al. (2002) proposed a new SVM method based on the least square method and called it the Least-Square Support Vector Machine (LSSVM). The LSSVM method helps to provide a time-saving advantage over the standard SVM, with the use of equality type constraints instead of inequalities (Suykens and Vandewalle, 1999). More information on LSSVM can be found in the publication by Suykens et al. (2002). The code of LSSVM was downloaded from the website http://www.esat.kuleuven.be/sista/lssvmlab/.

3.4. The SWAT model

The SWAT (Soil and Water Assessment Tool) model is a result of nearly 30 years of modeling efforts conducted by the USDA Agricultural Research Service (Arnold et al., 1998). It has gained international reputation as a robust interdisciplinary watershed modeling tool, as evidenced by numerous publications and series of international SWAT conferences. In SWAT, large watersheds are divided into sub-watersheds, which are then divided into Hydrologic Response Units (HRUs). A technical description of SWAT can be found in Neitsch et al. (2005). The model includes three main modules: hydrological process module, soil erosion module and pollution loading module.

In this study, we mainly used the hydrological process module, which is snowmelt- and rain-dependent. SWAT simulates snowmelt using the degree-day factor method. As the glacier module is lacking, this study treats glacier as snow. The model is normally run using daily measured meteorological data and parametrized using DEM (digital elevation model) data, land-use data and soil data. Readers can refer to the above-mentioned references for the detailed description of the model.

The parameters were calibrated following the criterion: first the upstream then downstream; water balance before other hydrological processes. The degree-day factor for snowmelt is calculated by a sinusoidal function to represent its seasonal change pattern with maximum and minimum values occurring on summer and winter solstices (Neitsch et al., 2005; Luo et al., 2013). The degree-day factors for snowmelt were calibrated based on the seasonal distribution and the magnitude of simulated streamflow. Since daily observed discharge was not available for the study, the streamflow was calibrated on the monthly scale.

3.5. Measures of performance assessment

Pearson's correlation coefficient (R), normalized mean square error (NMSE), root mean square error (RMSE), Nash–Sutcliffe efficiency (NSE), RMSE-observations standard deviation ratio (RSR) and the Percent Bias (PBIAS) were used as statistical indices to assess the performance of models in this study.

Pearson's correlation coefficient (R) describes the degree of collinearity between simulated and measured data. The correlation

Table 2
Correlation coefficient and partial correlation of predictors with streamflow.

Predictors	huss2	huss5	pr4	pr7	$pr4_{t-1}$	$pr8_{t-1}$	tmp3
Correlation coefficient	0.859	0.869	0.779	0.721	0.858	0.841	0.783
Partial correlation	−0.154	0.294	0.198	−0.112	0.178	0.113	−0.251
Predictors	vas1	vas2	vas8	hurs4	hurs7	$va500_{t-3}$	
Correlation coefficient	0.449	−0.499	−0.470	−0.470	−0.363	−0.570	
Partial correlation	−0.272	−0.171	0.100	−0.193	0.161	0.170	

Note: these predictors $pr4_{t-1}$ and $pr8_{t-1}$ donate lag 1 month. All significance value $p < .01$.

coefficient, which ranges from −1 to 1, is an index of the degree of linear relationship between the observed and simulated data. NMSE is the measure of the deviation between the actual and predicted values. The smaller the value of NMSE, the closer is the predicted time series values to the actual values. The Nash-Sutcliffe efficiency (NSE) is a normalized statistic that determines the relative magnitude of the residual variance compared to the measured data variance (Nash and Sutcliffe, 1970). NSE ranges between −∞ and 1.0 (1 inclusive), with NSE =1 being the ideal value. Values between 0.6 and 1.0 are generally viewed as an acceptable level of performance, whereas values < 0.0 mean that the average of observed values is a better predictor than the simulated values, which indicates a poor, unacceptable performance. RMSE-observations standard deviation ratio (RSR) is one of the commonly used error index statistics (Vazquez-Amabile and Engel, 2005). RSR standardizes RMSE using the standard deviation of observations, and it combines both an error index and additional information and is recommended to use by Legates and McCabe (1999). RSR is calculated as the ratio of the RMSE and standard deviation of measured data. Percent bias (PBIAS) measures the average tendency of the simulated data to be larger or smaller than their observed counterparts (Gupta et al., 1999). The general performance ratings for recommended statistics is described in Moriasi et al. (2007).

In hydrological modeling, the 95% confidence interval (CI) is usually used to guide the decision making in water resource management. Two coefficients were introduced to estimate the 95% uncertainty interval of the BNN model outputs: (1) the percentage of coverage (POC) of observations by the uncertainty interval, and (2) the average width (AW) of the uncertainty interval. Under the expected proportion, it is better when the POC is bigger. The average width $AW = \Sigma_{t=1}{}^{T}(Q_t{}^{u} - Q_t{}^{l})/T$, where $Q_t{}^{u}$ and $Q_t{}^{l}$ are the upper bound and the lower bound of the uncertainty interval at time t. Theoretically, when specified the POC, the uncertainty interval with smaller AW value is considered better.

In addition to the CI based evaluation, we also employed the continuous ranked probability score (CRPS) (Hersbach, 2000) and the predictive QQ plot (Laio and Tamea, 2007; Thyer et al., 2009) to evaluate the performance of the BNN model for continuous probabilistic forecasting. The minimum value 0 of CRPS denotes a perfect probabilistic simulation. The larger the CRPS value, the poorer performance. For the entire time period of model evaluation, the CRPS calculated for each value are averaged to obtain an overall indicator (Zhang et al., 2011). The predictive QQ plot (Laio and Tamea, 2007; Thyer et al., 2009) is a graphical tool to verify the goodness of fit of the probabilistic forecast. The details of the procedure are given by Laio and Tamea (2007). To conduct the test, the cumulative distribution function (CDF) of predicted streamflow at time t is evaluated. The probability integral transforms is $V_t = \int_{-\infty}{}^{x} f(x_t)dx$. Where $f(x_t)$ is the PDF of model outputs obtained from the uncertainty analysis (i.e., BNN simulations). If the probabilistic predictions of streamflow are suitable, the v_t values will be mutually independent and distributed uniformly between 0 and 1. To test uniformity, a probability plot can be employed to graphically examine how well the distribution of v_t values matches a $U(0,1)$ distribution. The condition of mutual independence can be tested using the standardized Kendall's τ_{st} statistics.

4. Results and discussions

4.1. Pre-analysis for predictors and reanalysis data

Predictor selection is of a great importance for the data-driven statistical models should be done carefully. In this study, the reanalysis grid cells (3 × 3 JRA55 grids) covering both the geographic area under study as well as the surrounding areas with meteorological influence on the Kaidu River were selected as the candidate grid cells for predictor variables. Each variable from Table 1 and its' lagged variables which lagged from one month to three months were included. This means that each grid cell "contained" 60 potential predictor variables. Based on stepwise regression approach (Cannon and Whitfield, 2002; Hessami et al., 2008; Chen et al., 2011), finally, 13 predictors were selected (Table 2) from the total 540 candidate predictor variables for model building. The results show that streamflow is sensitive to mean temperature at 2 m, precipitation and near surface specific humidity, which indicates that runoff in the Kaidu River is mainly influenced by climatic conditions defined jointly by precipitation, temperature and water vapor.

4.2. Inter-comparison of three approaches BNN, LSSVM and SWAT

The total data set (1979–2014) was divided into training and testing period, where the data (1979–2002) was used to train the developed model while the rest (2003–2014) was used for testing. To avoid some weights that were trained to be extremely large or small (in absolute value) to accommodate different scales of input and output variables, all input and output variables were normalized by *Z*-score method before feeding to BNN and LSSVM models. The model generalization capability and its accuracy depend on the quality of the training data. Further, outlier detection and their treatments also improve the accuracy of the statistical models (Gerlach et al., 1999). To make the developed model robust and effective to capture the unseen variability, four outliers were removed from the training period based on the output variable Z-score > 3.

For BNN model, to implement the EMC algorithm, we need to initialize the parameters used in BNN that control its effectiveness and efficiency. The iteration of EMC was set to 100,000, where the first 5000 iterations were used for the initialization process, following 10,000 iterations were discarded for the burn-in process, and the last 85,000 iterations were used for inference. We chose a prior on σ^2 by setting $\nu_1 = 0.05$, $\nu_2 = 0.5$ (Neal, 1996). Following Liang (2005), $\nu_3 = \nu_4 = 0.05$. Further, mutation rate $\eta = 0.6$, Metropolis step size $\kappa = 0.25$, the highest temperature $t_1 = 20$, the lowest temperature $t_N = 1$, and the intermediate temperatures equally spaced in inverse between t_1 and t_N as suggested by Liang (2005). The M and λ together control the network size of BNN. In this study, they were obtained by using 5-fold cross-validation procedure. Finally, hidden units $M = 3$ and hyper-parameter λ = 35. For LSSVM model, we set the optimization routine, cost function, kernel function and weight function to "simplex", "crossvalidatelssvm", "RBF_kernel" and "whuber", respectively. Besides, we also used 5-fold cross-validation procedure to determine the optimal hyper-parameter. Ultimately, the optimal regularization parameter γ = 498.84 and optimal kernel parameter $\sigma^2 = 261.49$.

Table 3
Evaluation of the performance of the LSSVM, BNN and SWAT for streamflow simulation.

Model	R	NSE	RSR	|PBIAS|	RMSE	NMSE	POC	AW	CRPS
Training									
BNN	0.91	0.83	0.42	0.03	27.06	11.25	69%	46.25 m^3/s	17.22
LSSVM	0.93	0.86	0.38	0	24.57	9.27			
SWAT	0.87	0.65	0.59	19.39	39.43	21.83			
Testing									
BNN	0.90	0.81	0.44	0.49	27.41	6.05	71%	49.71 m^3/s	17.15
LSSVM	0.89	0.80	0.45	1.42	28.16	6.69			
SWAT	0.71	0.57	0.65	19.74	51.25	22.62			

To illustrate the ability of BNN model to simulate streamflow plausibly, it is inter-compared with LSSVM and SWAT models. Table 3 shows the inter-comparison of performance of BNN, LSSVM and SWAT models in the training and testing periods. According to this Table, the R, NSE, RSR, NMSE and RMSE values for LSSVM model are better than for BNN in the training period. However, these five measures consistently indicate a better performance of BNN than LSSVM during the testing period. Usually, relative variations of RMSE is considered as a reference indicator to estimate the effectiveness of the trained model while capturing the overall variability of the true process. The analysis of RMSE values (Table 3) clearly indicates that BNN has a better generalization capacity than LSSVM.

Simultaneously, when comparing with SWAT, we can see that only correlation coefficient is close to that of BNN in the training period. However, the BNN model performs much better in terms of the key criteria (NSE, RMSE, NMSE and PBIAS), whereas those of SWAT are only acceptable (Moriasi et al., 2007). In the testing period, the performance of SWAT decreases significantly. Since hydrological models are better characterized at finer time scales, in this study, transforming the daily simulated streamflow into monthly will arouse extra uncertainties. Still, it doesn't affect the conclusion that SWAT model does not possess a better prediction capacity compared to BNN. This is due to a high heterogeneity of mountain meteorology in the Kaidu River basin in combination with poor available climate and geospatial data. But 41 parameters need to be calibrated for SWAT model, which is a hard work. This introduces the main uncertainties to the simulation. Moreover, statistical hydrological models are superior to physical-based hydrological models for prediction have confirmed by earlier studies (Khan and Coulibaly, 2006; Demirel et al., 2009; Kim et al., 2012). For example, Kim et al. (2012) pointed out that ANN can provide more accurate monthly prediction than SWAT. Anyway, physical-based hydrological model specializes in an understanding of the physical processes, however, when prediction accuracy becomes the main concern, the statistical hydrological model can be a good model alternative (Khan and Coulibaly, 2006).

A comparison of observed and simulated monthly streamflows for all three models (BNN, LSSVM, SWAT) in the training and testing periods is represented in Fig. 4. It can be seen that simulations of both BNN and LSSVM are closer to the observed data than those of SWAT. However, it also shows that the statistical models usually underestimate high values. This is consistent with the finding by Fowler et al. (2007) that statistical model tends to underestimate variance and poorly represent extreme high values, which probably is the inborn defect of statistical model. What's more, the high values may be caused by extreme precipitation or glacial lakes bursting in a short time in summer, which can't be captured by JRA55 reanalysis data. Thus, the models also fail to accurately capture the extreme streamflow when using JRA55 reanalysis data as inputs. Thirdly, coarse spatial resolution of the reanalysis dataset probably is another main reason. Still, statistical models (BNN and LSSVM) are superior to the physically based hydrological model (SWAT) in such a data sparse alpine region at monthly scale.

Furthermore, statistical evaluation coefficients were calculated to evaluate the performance of the BNN model for uncertainty estimation, as shown in Table 3. To estimate the uncertainty of BNN, totally 100, 000 iterations were implemented by driving the EMC method according to the posterior probability distribution of BNN. A total of 85, 000 samples were finally picked out after eliminating the samples from the burning period, and then the network outputs were calculated. From Table 3 we can see that POC and AW change only slightly in the training period compared to the testing period, indicating a good generalization ability in the predictive uncertainty estimation. The median of simulation outputs and 95% uncertainty intervals estimated by the BNN model are shown in Fig. 5. It can be seen that the 95% uncertainty intervals contain most of observed values, except for several extremes. However, from Table 3 we find that the AWs are still large. The reason may be that the BNN model only take parameters uncertainty and structure uncertainty into consideration, except the inputs uncertainty. Furthermore, it is likely due to some other important factors are not considered in this study, such as ground water, soil moisture, glacier- and snow-melt, which is the obviously drawback of BNN. Thus, to improve the uncertainty estimation capacity of BNN, effective methods for considering the uncertainties associated with input hydrometeorological data (e.g., Srivastav et al., 2007) and observed outputs

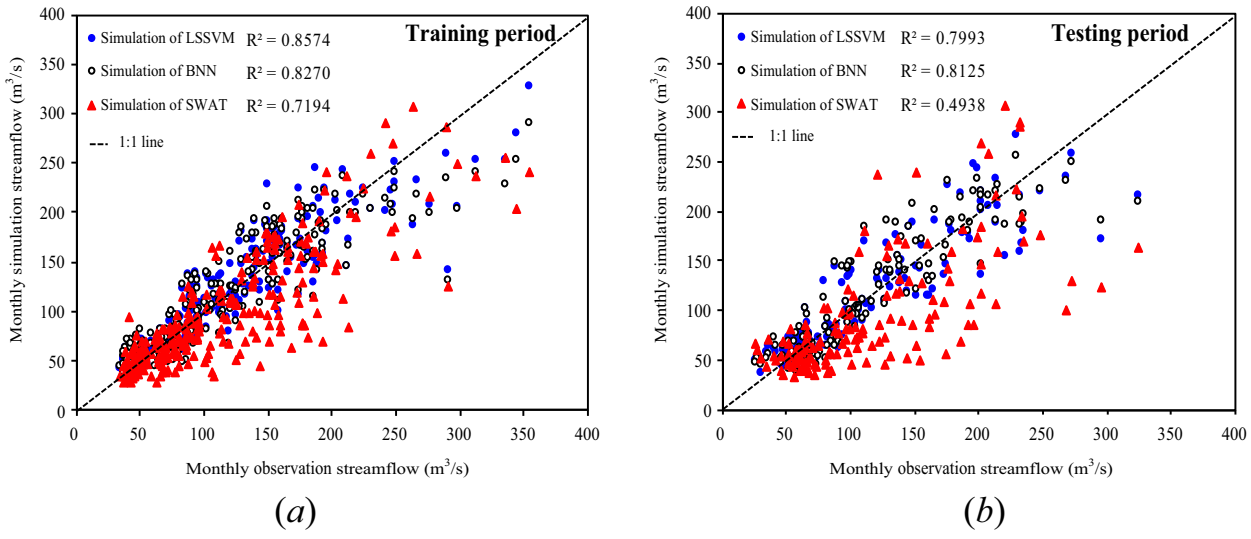

Fig. 4. Scatter plot between the observed and predicted monthly streamflow in both the calibration period (left) and validation period (right).

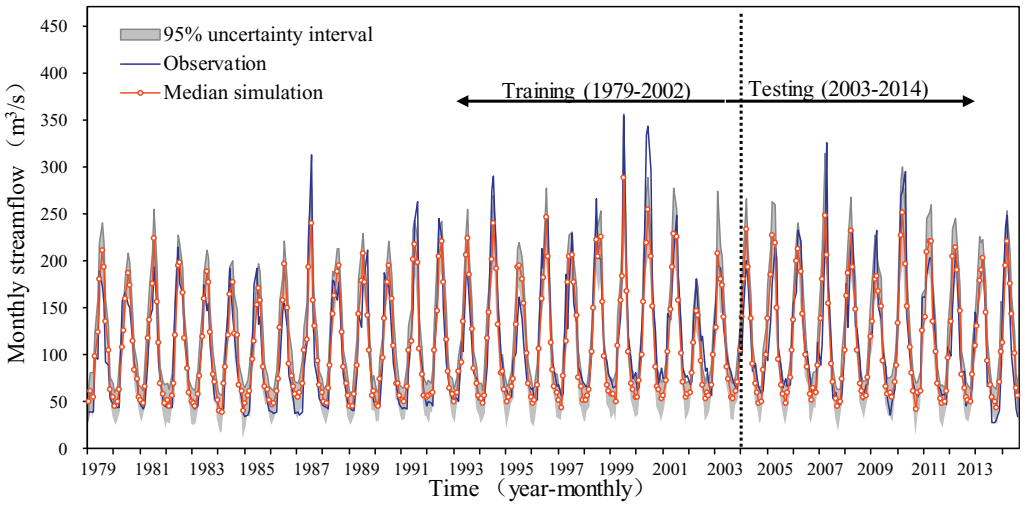

Fig. 5. Observed, BNN modeled monthly streamflow and 95% uncertainty interval.

must be considered in the definition of posterior model probability. More variables should also be taken into consideration to remedy the limitation of the BNN approach that can't reflect the impacts of land use change and don't include hydrological process.

Further analysis using CRPS (Table 3) and the predictive QQ plot with respect to the probability plot of v_t values versus a theoretical uniform distribution is shown in Fig. 6, along with the Kolmogorov confidence bands at the 95% confidence level. From Table 3, we can see that CRPS in the testing period is only slightly different compared to the training period. Fig. 6 shows that the distribution of v_t values matches that of a $U(0,1)$ distribution very well in the testing period, satisfying the first condition of the test. In addition, the condition of mutual independence was met under the standardized Kendall's τ_{st} statistic ($\tau_{st} = 1.41 < 1.645$), satisfying the second condition of the test. These results confirm that predictions of streamflow by the BNN probabilistic model are reliable.

All the above suggests that BNN is capable of generating robust runoff projections. The reasons supporting it are summarized below. First of all, the structure of BNN is variable, which adopted a technique called "dropout" (Srivastava et al., 2014) can effectively prevent overfitting and reduce dependence the initial specification for the input patterns and the number of hidden units. This means that potential predictors with a low correlation to streamflow would be not assigned to the model. Only predictors with a high correlation are linked via active connections. The factors that are not assigned to active connections can be omitted. Besides, the inputs are selected automatically by the EMC methods (Liang, 2005) sampling from the joint posterior of the network structure and weights. Multiple sampling can generate considerable different BNN models. Further, the structural difference between various BNN models covers most of the variability in the data set and when the results are averaged, it decreases the over-fitting tendency of the developed model. While the single LSSVM model can't overcome the over-fitting problem. Thirdly, the combination of variable model structure and EMC sampling technique provide a more reasonable quantification of uncertainty of streamflow simulation compared to the fixed model structure employed in Khan and Coulibaly (2010) and help to obtain a larger POC (i.e. percentage of observations within the interval). Therefore, BNN is suitable for streamflow prediction in this study.

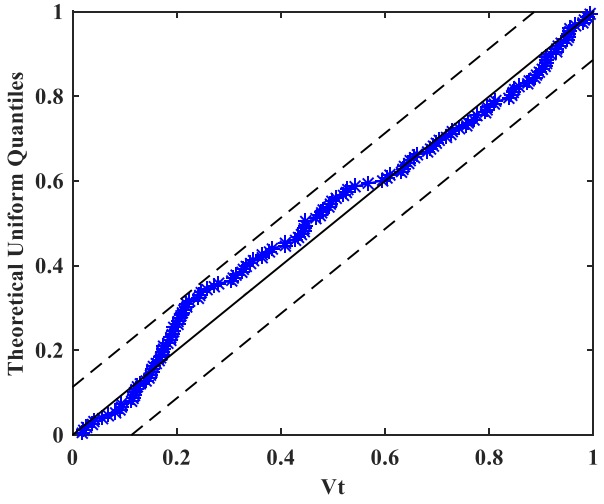

Fig. 6. Q-Q plot of the sample quantiles of the v_t values versus those of a U(0,1) distribution for validation period of BNN. Kolmogorov confidence bands (dashed lines) at the 95% confidence level are also shown.

4.3. Future streamflow scenarios

The future streamflow scenarios were constructed using the consolidated model over three-time horizons 2020s (2017–2039), 2050s (2040–2069) and 2080s (2070–2099). 1980–2009 is used as a baseline. The monthly streamflow (2017–2099) is projected under three emission scenarios (RCP2.6, RCP4.5 and RCP8.5) using the outputs of five latest bias-corrected GCMs. Fig. 7 shows the annual streamflow projected for the future. Quite significant increases were found under RCP8.5 by the end of 21th century. The long-term average annual streamflow is projected to increase by 9.12%, 15.33% and 21.04% at 2020s, 2050s, 2080s, correspondingly.

By analyzing seasonal variation of streamflow, different change patterns can be found in four seasons (Fig. 8). Mostly increases in spring, winter and autumn, however slight variations can be observed in summer. Streamflow in spring shows a consistent increase in the future under all three emission scenarios. In general, increases under the RCP2.6 scenario are less significant than those under the RCP4.5 scenario, and the most prominent increases are found under the RCP8.5 scenario. The seasonal streamflow variation in autumn and winter, shows the similar patterns as was in spring, however with different amplitude of variations under the corresponding RCPs. These changes in summer streamflow are different. Streamflow tends to slightly decrease under RCP2.6, and it increase under RCP4.5 and RCP8.5 in all three periods. Summer streamflow is projected to have significant increase in the third period under RCP8.5.

Fig. 9 illustrates the intra-annual change for the basin. The average

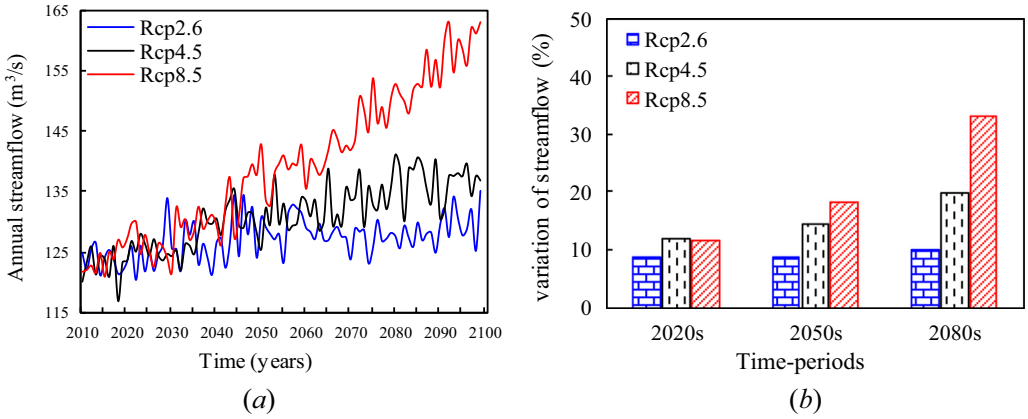

Fig. 7. Projected future streamflow using BNN based model (*a*); Projected variation between the base period (1980–2009) and the three future periods under the RCPs scenarios (*b*).

variations of the monthly streamflow are 16.39%, 22.17% and 28.01% during 2020s, 2050s and 2080s, respectively. We can also see that the peak value gradually increases from 2020s to 2080s. It is noteworthy that the most remarkable increase appears in March, with averaged amplitudes of about 59.84%, 68.32% and 76.11% during 2020s, 2050s and 2080s, respectively. This may be due to increase of snowmelt in this month. In March, the Kaidu River flow is mainly fed by snowmelt. With an increase in temperature under global warming, the mountain snow will thaw with a higher speed, leading to a sharp increase in streamflow.

In summary, climate change is expected to change the streamflow magnitude and duration. It is likely that the spring runoff would increase, and the summer runoff would decrease, which could lead to reallocation of water resources and alteration of the fragile ecological environment in the downstream oases.

4.4. Uncertainty analysis

The reasonable estimates of predictive uncertainty of hydrologic prediction are valuable to water resources and environmental management (Liu and Gupta, 2007). Both overestimation and underestimation of uncertainty can lead to imperfect preparation to potential situations. The errors in input data and model structure and parameters of hydrological models collectively introduce large uncertainty. Thus, uncertainty estimation is essential, especially for streamflow projection. Table 4 shows statistical evaluation coefficients of 95% uncertainty intervals for three future projection periods (2017–2099) under three RCPs for the monthly streamflow. When comparing the Average Widths (AWs) in Table 4 between all the three periods of projection, we find not too many changes except for RCP8.5 at the end of 21th century. However, there is a big difference between the AWs in Table 4 and Table 3. This suggests that inputs could bring a large uncertainty, which should be taken into consideration, especially for the streamflow

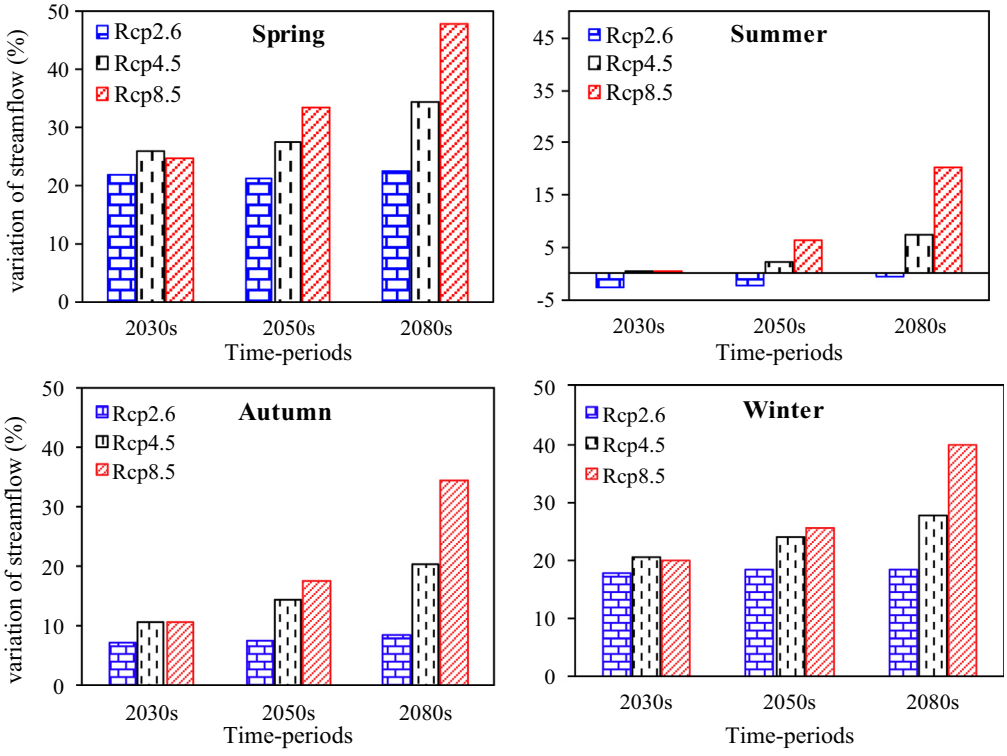

Fig. 8. Average season changes in streamflow between baseline period (1980–2009) and the future three periods under the RCPs.

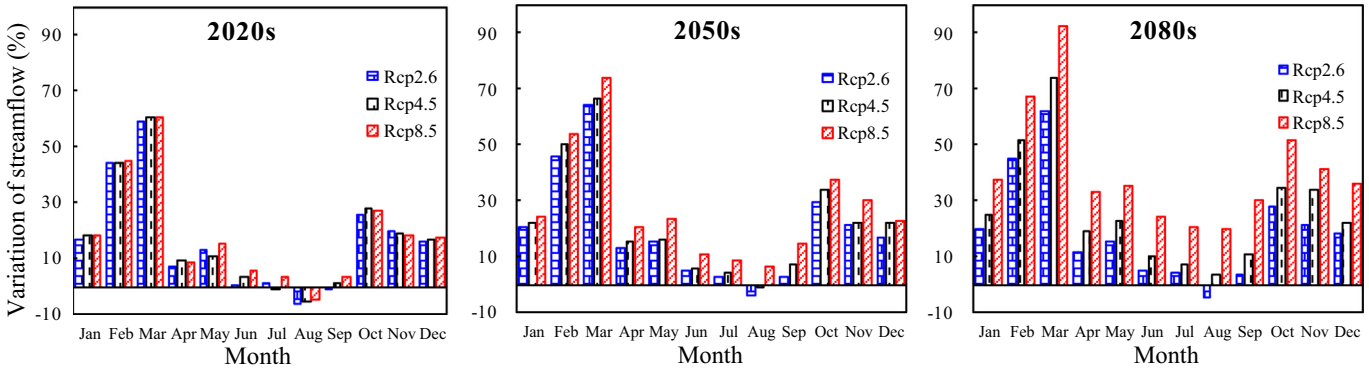

Fig. 9. Average monthly changes in streamflow between the baseline period (1980–2009) and the three periods under RCPs.

Table 4
Statistical evaluation coefficients of BNN for uncertainty intervals AW (m^3/s) during three projection periods under RCPs.

Scenarios	Projection		
	2020s	2050s	2080s
RCP26	83.96	85.60	85.75
RCP45	83.72	87.02	88.85
RCP85	85.63	91.18	99.64

projection under GCMs.

AWs of the 95% confidence intervals of the annual and mean monthly streamflow projections under three RCPs scenarios are presented in Fig. 10. As can be seen that all AWs under three RCPs scenarios show consistent increases until the end of 21st century. The most prominent increase of AW is found under the RCP8.5 scenario, followed by the RCP4.5 scenario, and the increase in AW under the RCP2.6 scenario is relatively small. Regarding AW of the average monthly streamflow in Fig. 10b, the average largest AW appears in July (116.05 m^3/s), and the lowest in January (49.55 m^3/s). It suggests that AW would increase with the volume of runoff.

4.5. Prospect and discussion

To illustrate the data insufficiency issue over the world high-elevation mountain areas, the meteorological sites information (http://www.ncdc.noaa.gov/homr/reports) of the world is used for analysis. The classification by the United Nations Environment Programme - World Conservation Monitoring Centre (UNEP-WCMC, 2002) is: low altitude region (< 1000 m), mid-altitude region (1000–2500 m), sub-high altitude region (2500–4000 m), and high altitude region (> 4000 m). Fig. 11 suggests that meteorological stations density decreases rapidly with increasing elevation. WMO recommended that the minimum density for plain and hill should be 5750 km^2/station, while, for mountains, the minimum density should be 2500 km^2/station due to large spatial heterogeneity of precipitation and other weather parameters. (WMO, 2008). The analysis indicates that meteorological station density of low altitude region (1.84 stations/5750 Km^2 = 3125 km^2/station) and mid-altitude region (0.98 stations/5750 Km^2 = 5867 km^2/station) can meet the basic needs. However, it is seriously data-limited for both sub-high altitude regions (13,888 km^2/station) and high altitude regions (50,000 km^2/station), which are called alpine regions in this study.

Currently, the degree-day model is a widely used method for glacier and snow melt computation (Lutz et al., 2014; Luo et al., 2013). Nevertheless, the model has obvious regional characteristics. For example, temperature is calculated by average temperature gradient method in data-sparse alpine regions, but the significant temporal-spatial variability of temperature lapse rate makes it hard to quantify parameters. This means that the degree-day method working under data limited conditions will introduce substantial uncertainties into hydrological modeling. Lutz et al. (2014) simulated High Asia's eight rivers using Spatial Processes in Hydrology model based on the degree-day model, the results showed that the Nash-Sutcliffe criterion in the validation period was only 0.39 at the Dainyor bridge station, which it not satisfactory (Moriasi et al., 2007). Whereas, the consolidated streamflow projection model directly from GCMs based on BNN built in this study requires less data (only reanalysis and runoff data) than a

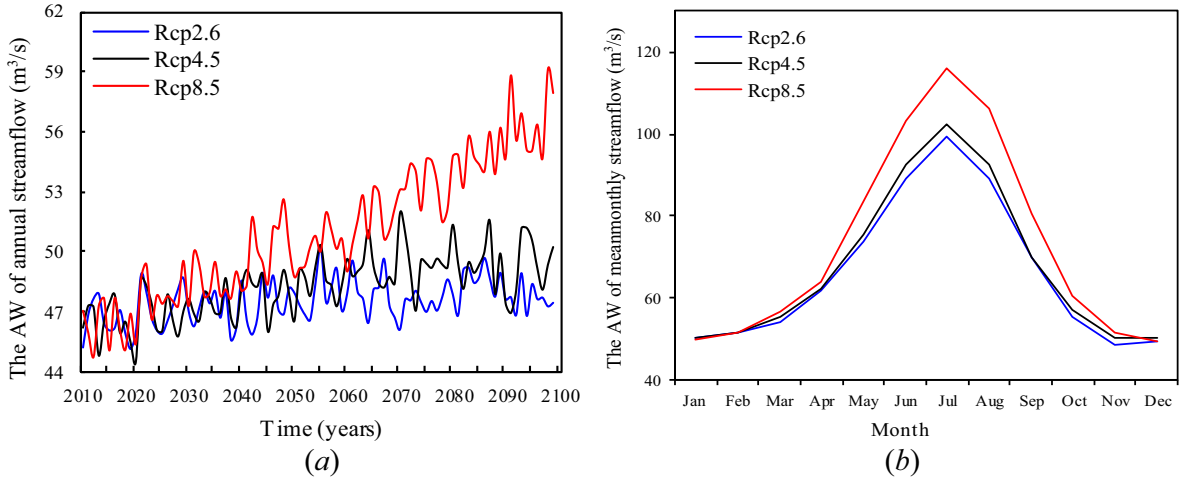

Fig. 10. The AWs of streamflow under RCPs scenarios (*a*) annual during 2017–2099 and (*b*) average monthly.

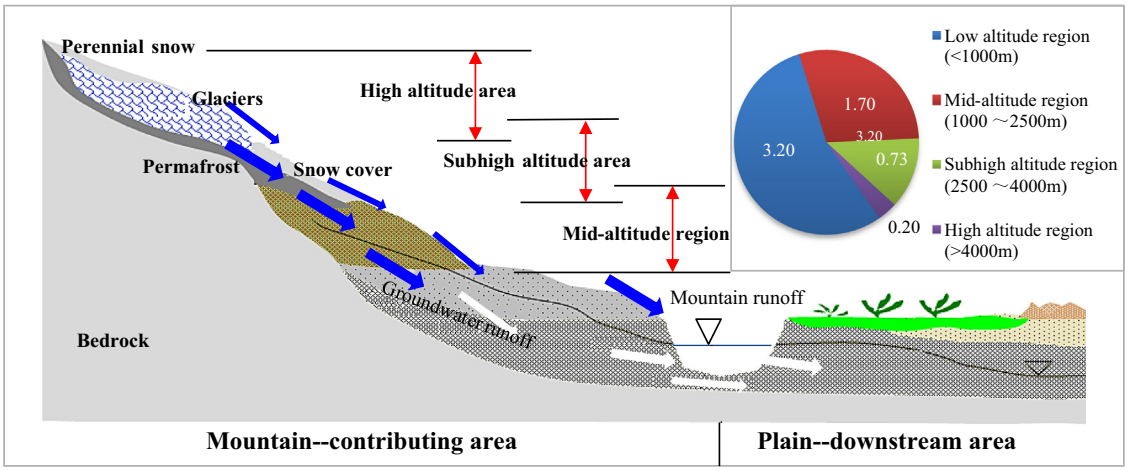

Fig. 11. Illustration for high mountain hydrological processes and weather stations density of different regions (station/10,000 Km^2).

conventional hydrological model (e.g., DEM, land use, vegetation, soil, temperature, rainfall). Besides, the BNN model has a robust generalization ability, which could provide more reliable streamflow projection.

This work is different with the previous studies (e.g. Khan and Coulibaly, 2010) in the following aspects:

(1) The focus of previous relevant studies was to estimate uncertainties through a probabilistic approach by BNN. Whereas, the goal of our work was to construct a more direct and effective way to evaluate the climate impact on streamflow omitting the conventional steps of downscaling and hydrological modeling in the data-sparse regions.

(2) The BNN approach is hereby more advanced. The structure of BNN is variable, which could generate more probable results so as to obtain a larger POC, which providing more reasonable quantification of the uncertainty of streamflow simulation than that by a fixed model structure employed in previous studies (Khan and Coulibaly, 2010; Khan and Coulibaly, 2006). What's more, the structure of BNN model is usually much sparse and less depending on the initial specification for the input patterns and the number of hidden units, which works well in the data-sparse regions. In addition, a more effective evolutionary Monte Carlo (EMC) algorithm was used to train the BNN model. It can help to avoid the local convergence commonly encountered in training, therefor it is more effective than the MCMC methods commonly employed in the past.

(3) To overcome the huge uncertainties existing in the old GCMs, we used the latest bias-corrected GCMs (HadGEM2-ES, MIROC-ESM-CHEM, NorESM1-M, IPSL-CM5A-LR and GFDL-ESM2M) with grid resolution of 0.5° provided by the Inter-Sectoral Impact Model Intercomparison Project (ISI-MIP) (Hempel et al., 2013). RCPs, widely adopted by IPCC for generation of climate model results for the fifth IPCC Assessment Report (AR5), have been included to identify impacts of concentrations of a variety of greenhouse gases, as well as land-use, air pollution, changes in technology, population, energy production and a variety of additional factors. This can help to generate more confident projections. On the other hand, the SDSM downscaling used to derive local-scale meteorological data from GCMs is omitted in our work. Reducing the redundant downscaling may decrease uncertainty to some degree.

(4) To date, there are many reanalysis data (e.g. NCEP-NCAR, JRA55, JRA25, MERRA, ERA-interim) publicly released by different research communities for climate research. The reanalysis data also has important influences on the final results, but they have not been thoroughly analyzed before (Huang et al., 2016; Hodges et al., 2011). After a careful inter-comparison (Table S1), JRA-55 was identified and used in our study. This also could help to reduce related uncertainties.

The above four aspects collectively constitute the distinctive deliverables to provide beneficial insights in directly simulating and projecting streamflow under climate change and explain why our work has a great significance for the data sparse regions.

5. Conclusions

This study presented a probabilistic streamflow projection approach, which was applied using the latest GCM outputs in a data sparse alpine region, the Kaidu River basin in Central Asia. An advanced BNN with flexible structures was used to build the model forced by large scale climate predictor variables. The major findings can be summarized as follows:

1) The BNN model is superior to the stochastic model (LSSVM) and the process-based hydrological model (SWAT) in the data sparse alpine region. Besides, it enables to provide a more reliable streamflow projection for a robust generalization ability, which leads to a promising potential compared to the traditional hydrological models that highly depend on a range of geographical, meteorological and hydrological data and involve a series of complex procedures for application.
2) The long-term average annual streamflow in Kaidu River is expected to increase in the 21th century, especially under the RCP8.5 emission scenario. Besides, the streamflow is projected to change diversely in different seasons which would increase in spring and autumn but decrease in summer. Most importantly, a remarkable increase is likely to appear in March.
3) By considering variable model structure and informative prior knowledge, the BNN model can provide a relative good performance of the uncertainty of streamflow simulation. But the use of GCMs for BNN is connected with a large uncertainty, which should be taken into account. Besides, uncertainties in projections would probably increase with time.
4) Most alpine regions above 2500 m across the world have limited meteorological observation networks which seriously restricts evaluation of climate change impacts on water resource and streamflow projection using conventional hydrological model approaches. The proposed probabilistic projection approach in this study can work as a potentially powerful alternative to the conventional methods in runoff predictions of these alpine regions.

Acknowledgments

The work was jointly supported by the grants from the National Natural Science Foundation of China (41561134016.), a key grant of Chinese Academy of Sciences (KZZD-EW-12) and a grant from the

Ministry of Education (2015B25714). Authors would like to thank Valentina Krysanova from the Potsdam Institute for Climate Impact Research for her constructive suggestions. The authors are grateful to the editors and the anonymous reviewers for their insightful comments and suggestions.

Appendix A. Supplementary data

Supplementary data to this article can be found online at https://doi.org/10.1016/j.gloplacha.2018.03.011.

References

Anandhi, A., Srinivas, V.V., Nanjundiah, R.S., Kumar, D.N., 2008. Downscaling precipitation to river basin in India for IPCCSRES scenarios using support vector machine. Int. J. Climatol. 28 (3), 401–420. http://dx.doi.org/10.1002/joc.1529.

Arnold, J.G., Srinivasan, R., Muttiah, R.S., Williams, J.R., 1998. Large area hydrologic modeling and assessment - part 1: model development. J. Am. Water Resour. Assoc. 34 (1), 73–89. http://dx.doi.org/10.1111/j.1752-1688.1998.tb05961.x.

Bates, B.C., Charles, S.P., Hughes, J.P., 1998. Stochastic downscaling of numerical climate model simulations. Environ. Model Softw. 13 (3–4), 325–331. http://dx.doi.org/10.1016/s1364-8152(98)00037-1.

Beam, A.L., Motsinger-Reif, A., Doyle, J., 2014. Bayesian neural networks for detecting epistasis in genetic association studies. Bmc Bioinformatics 15, 12. http://dx.doi.org/10.1186/s12859-014-0368-0.

Cannon, A.J., Whitfield, P.H., 2002. Downscaling recent streamflow conditions in British Columbia, Canada using ensemble neural network models. J. Hydrol. 259 (1–4), 136–151. http://dx.doi.org/10.1016/s0022-1694(01)00581-9.

Chen, J., Brissette, F.P., Leconte, R., 2011. Uncertainty of downscaling method in quantifying the impact of climate change on hydrology. J. Hydrol. 401 (3–4), 190–202. http://dx.doi.org/10.1016/j.jhydrol.2011.02.020.

Chen, X., Yang, T., Wang, X., Xu, C.-Y., Yu, Z., 2013. Uncertainty intercomparison of different hydrological models in simulating extreme flows. Water Resour. Manag. 27 (5), 1393–1409. http://dx.doi.org/10.1007/s11269-012-0244-5.

Dai, X., Li, W., Ma, Z., Wang, P., 2007. Water-vapor source shift of Xinjiang region during the recent twenty years. Prog. Nat. Sci. 17 (5), 569–575.

Demirel, M.C., Venancio, A., Kahya, E., 2009. Flow forecast by swat model and ann in pracana basin, Portugal. Adv. Eng. Softw. 40 (7), 467–473.

Dickerson-Lange, S.E., Mitchell, R., 2014. Modeling the effects of climate change projections on streamflow in the Nooksack River basin, Northwest Washington. Hydrol. Process. 28 (20), 5236–5250. http://dx.doi.org/10.1002/hyp.10012.

Ebita, A., et al., 2011. The Japanese 55-year reanalysis "JRA-55": an interim report. Sola 7, 149–152. http://dx.doi.org/10.2151/sola.2011-038.

Fowler, H.J., Blenkinsop, S., Tebaldi, C., 2007. Linking climate change modelling to impacts studies: recent advances in downscaling techniques for hydrological modelling. Int. J. Climatol. 27 (12), 1547–1578. http://dx.doi.org/10.1002/joc.1556.

Gao, C., Gemmer, M., Zeng, X., Liu, B., Su, B., Wen, Y., 2010. Projected streamflow in the Huaihe River Basin (2010−2100) using artificial neural network. Stoch. Env. Res. Risk A. 24 (5), 685–697. http://dx.doi.org/10.1007/s00477-009-0355-6.

Gerlach, G., Carter, C.K., Kohn, R., 1999. Diagnostics for time series analysis. J. Time Ser. Anal. 20 (3), 309–330.

Ghosh, S., Mujumdar, P.P., 2008. Statistical downscaling of GCM simulations to streamflow using relevance vector machine. Adv. Water Resour. 31 (1), 132–146. http://dx.doi.org/10.1016/j.advwatres.2007.07.005.

Gupta, H.V., Sorooshian, S., Yapo, P.O., 1999. Status of automatic calibration for hydrologic models: comparison with multilevel expert calibration. J. Hydrol. Eng. 4 (2), 135–143. http://dx.doi.org/10.1061/(asce)1084-0699(1999)4:2(135).

Hempel, S., Frieler, K., Warszawski, L., Schewe, J., Piontek, F., 2013. A trend-preserving bias correction - the ISI-MIP approach. Earth System Dynamics 4 (2), 219–236. http://dx.doi.org/10.5194/esd-4-219-2013.

Hersbach, H., 2000. Decomposition of the continuous ranked probability score for ensemble prediction systems. Weather Forecast. 15 (5), 559–570. http://dx.doi.org/10.1175/1520-0434(2000)015<0559:dotcrp>2.0.co;2.

Hessami, M., Gachon, P., Ouarda, T.B.M.J., St-Hilaire, A., 2008. Automated regression-based statistical downscaling tool. Environ. Model Softw. 23 (6), 813–834. http://dx.doi.org/10.1016/j.envsoft.2007.10.004.

Hodges, K.I., Lee, R.W., Bengtsson, L., 2011. A comparison of extratropical cyclones in recent reanalyses ERA-interim, NASA MERRA, NCEP CFSR, and JRA-25. J. Clim. 24 (18), 4888–4906. http://dx.doi.org/10.1175/2011jcli4097.1.

Huang, D.-Q., Zhu, J., Zhang, Y.-C., Huang, Y., Kuang, X.-Y., 2016. Assessment of summer monsoon precipitation derived from five reanalysis datasets over East Asia. Q. J. R. Meteorol. Soc. 142 (694), 108–119. http://dx.doi.org/10.1002/qj.2634.

IPCC5, 2013. Summary for policymakers. In: Stocker, T.F., Qin, D., Plattner, G.K., Tignor, M., Allen, S.K., Boschung, J., Nauels, A., Xia, Y., Bex, V., Midgley, P.M. (Eds.), Climate Change 2013: The Physical Science Basis. Contribution of Working Group I to the Fifth Assessment Report of the Intergovernmental Panel on Climate Change. Cambridge University Press, Cambridge. United Kingdom and New York. NY, USA.

Kalra, A., Ahmad, S., 2012. Estimating annual precipitation for the Colorado River Basin using oceanic-atmospheric oscillations. Water Resour. Res. 48. http://dx.doi.org/10.1029/2011wr010667.

Kanamitsu, M., Ebisuzaki, W., Woollen, J., Yang, S.K., Hnilo, J.J., Fiorino, M., Potter, G.L., 2002. NCEP-DOE AMIP-II reanalysis (R-2). Bull. Am. Meteorol. Soc. 83 (11), 1631–1643. http://dx.doi.org/10.1175/bams-83-11-1631.

Khan, M.S., Coulibaly, P., 2006. Bayesian neural network for rainfall-runoff modeling. Water Resour. Res. 42 (7). http://dx.doi.org/10.1029/2005wr003971.

Khan, M.S., Coulibaly, P., 2010. Assessing hydrologic impact of climate change with uncertainty estimates: BAYESIAN neural network approach. J. Hydrometeorol. 11 (2), 482–495. http://dx.doi.org/10.1175/2009jhm1160.1.

Kim, R.J., Loucks, D.P., Stedinger, J.R., 2012. Artificial neural network models of watershed nutrient loading. Water Resour. Manag. 26 (10), 2781–2797.

Laio, F., Tamea, S., 2007. Verification tools for probabilistic forecasts of continuous hydrological variables. Hydrol. Earth Syst. Sci. 11 (4), 1267–1277. http://dx.doi.org/10.5194/hess-11-1267-2007.

Landman, W.A., Mason, S.J., Tyson, P.D., Tennant, W.J., 2001. Statistical downscaling of GCM simulations to streamflow. J. Hydrol. 252 (1–4), 221–236. http://dx.doi.org/10.1016/s0022-1694(01)00457-7.

Legates, D.R., McCabe, G.J., 1999. Evaluating the use of "goodness-of-fit" measures in hydrologic and hydroclimatic model validation. Water Resour. Res. 35 (1), 233–241. http://dx.doi.org/10.1029/1998wr900018.

Liang, F.M., 2005. Bayesian neural networks for nonlinear time series forecasting. Stat. Comput. 15 (1), 13–29. http://dx.doi.org/10.1007/s11222-005-4786-8.

Liang, F., Kuk, Y.C.A., 2004. A finite population estimation study with Bayesian neural networks. Survey Methodology. 30, 219–234.

Liang, F.M., Wong, W.H., 2001. Real-parameter evolutionary Monte Carlo with applications to Bayesian mixture models. J. Am. Stat. Assoc. 96 (454), 653–666. http://dx.doi.org/10.1198/016214501753168325.

Liu, Y., Gupta, H.V., 2007. Uncertainty in hydrologic modeling: toward an integrated data assimilation framework. Water Resour. Res. 43 (7). http://dx.doi.org/10.1029/2006wr005756.

Liu, Z., Xu, Z., Charles, S.P., Fu, G., Liu, L., 2011. Evaluation of two statistical downscaling models for daily precipitation over an arid basin in China. Int. J. Climatol. 31 (13), 2006–2020. http://dx.doi.org/10.1002/joc.2211.

Luo, Y., Arnold, J., Liu, S., Wang, X., Chen, X., 2013. Inclusion of glacier processes for distributed hydrological modeling at basin scale with application to a watershed in Tianshan Mountains, northwest China. J. Hydrol. 477, 72–85. http://dx.doi.org/10.1016/j.jhydrol.2012.11.005.

Lutz, A.F., Immerzeel, W.W., Shrestha, A.B., Bierkens, M.F.P., 2014. Consistent increase in High Asia's runoff due to increasing glacier melt and precipitation. Nat. Clim. Chang. 4 (7), 587–592. http://dx.doi.org/10.1038/nclimate2237.

Moriasi, D.N., Arnold, J.G., Van Liew, M.W., Bingner, R.L., Harmel, R.D., Veith, T.L., 2007. Model evaluation guidelines for systematic quantification of accuracy in watershed simulations. Trans. ASABE 50 (3), 885–900.

Nash, J.E., Sutcliffe, J.V., 1970. River flow forecasting through conceptual models: part 1. A discussion of principles. J. Hydrol. 10 (3), 282–290.

Neal, R.M., 1996. Bayesian Learning for Neural Networks. Springer-Verlag, New York.

Neitsch, S.L., Arnold, J.G., Kiniry, J.R., Williams, J.R., King, K.W., 2005. Soil and Water Assessment Tool Theoretical Documentation: Version. Texas Water Resources Institute. College Station, TX, pp. 2005.

Niu, D.-x., Shi, H.-f., Wu, D.D., 2012. Short-term load forecasting using bayesian neural networks learned by Hybrid Monte Carlo algorithm. Appl. Soft Comput. 12 (6), 1822–1827. http://dx.doi.org/10.1016/j.asoc.2011.07.001.

Okkan, U., Inan, G., 2015. Statistical downscaling of monthly reservoir inflows for Kemer watershed in Turkey: use of machine learning methods, multiple GCMs and emission scenarios. Int. J. Climatol. 35 (11), 3274–3295. http://dx.doi.org/10.1002/joc.4206.

Okkan, U., Serbes, Z.A., Samui, P., 2014. Relevance vector machines approach for long-term flow prediction. Neural Computing & Applications 25 (6), 1393–1405. http://dx.doi.org/10.1007/s00521-014-1626-9.

Qian, W.H., Qin, A., 2008. Precipitation division and climate shift in China from 1960 to 2000. Theor. Appl. Climatol. 93 (1–2), 1–17. http://dx.doi.org/10.1007/s00704-007-0330-4.

Sachindra, D.A., Huang, F., Barton, A., Perera, B.J.C., 2013. Least square support vector and multi-linear regression for statistically downscaling general circulation model outputs to catchment streamflows. Int. J. Climatol. 33 (5), 1087–1106. http://dx.doi.org/10.1002/joc.3493.

Sachindra, D.A., Huang, F., Barton, A., Perera, B.J.C., 2015. Potential improvements to statistical downscaling of general circulation model outputs to catchment streamflows with downscaled precipitation and evaporation. Theor. Appl. Climatol. 122 (1–2), 159–179. http://dx.doi.org/10.1007/s00704-014-1288-7.

Shen, Y., Su, H., Wang, G., Mao, W., Wang, S., Han, P., Wang, N., Li, Z., 2013. The responses of glaciers and snow cover to climate change in Xinjiang (II): hazards effects. J. Glaciol. Geocryol. 35 (6), 1355–1370.

Shi, P., Yang, T., Zhang, K., Tang, Q., Yu, Z., Zhou, X., 2016. Large-scale climate patterns and precipitation in an arid endorheic region: linkage and underlying mechanism. Environ. Res. Lett. 11 (4). http://dx.doi.org/10.1088/1748-9326/11/4/044006.

Shi, P., Yang, T., Xu, C.-Y., Yong, B., Shao, Q., Li, Z., Wang, X., Zhou, X., Li, S., 2017. How do the multiple large-scale climate oscillations trigger extreme precipitation? Glob. Planet. Chang. 157, 48–58. http://dx.doi.org/10.1016/j.gloplacha.2017.08.014.

Srivastav, R.K., Sudheer, K.P., Chaubey, I., 2007. A simplified approach to quantifying predictive and parametric uncertainty in artificial neural network hydrologic models. Water Resour. Res. 43 (10). http://dx.doi.org/10.1029/2006wr005352.

Srivastava, N., Hinton, G., Krizhevsky, A., Sutskever, I., Salakhutdinov, R., 2014. Dropout: a simple way to prevent neural networks from overfitting. J. Mach. Learn. Res. 15, 1929–1958.

Suykens, J.A.K., Vandewalle, J., 1999. Least squares support vector machine classifiers. Neural. Process. Lett. 9 (3), 293–300. http://dx.doi.org/10.1023/a:1018628609742.

Suykens, J.A.K., Gestel, T.V., Brabanter, J.D., Moor, B.D., Vandewalle, J., 2002. Least Square Support Vector Machines. World Scientific, Singapore.

Tao, H., Wang, G., Shao, C., Song, Y., Zou, S., 2007. Climate change and its effects on

runoff at the headwater of Kaidu River. J. Glaciol. Geocryol. 29 (3), 413–417.
Taylor, K.E., Stouffer, R.J., Meehl, G.A., 2012. An overview of CMIP5 and the experiment design. Bull. Am. Meteorol. Soc. 93 (4), 485–498. http://dx.doi.org/10.1175/bams-d-11-00094.1.
Thyer, M., Renard, B., Kavetski, D., Kuczera, G., Franks, S.W., Srikanthan, S., 2009. Critical evaluation of parameter consistency and predictive uncertainty in hydrological modeling: a case study using Bayesian total error analysis. Water Resour. Res. 45. http://dx.doi.org/10.1029/2008wr006825.
Tisseuil, C., Vrac, M., Lek, S., Wade, A.J., 2010. Statistical downscaling of river flows. J. Hydrol. 385 (1–4), 279–291. http://dx.doi.org/10.1016/j.jhydrol.2010.02.030.
UNEP-WCMC, 2002. Mountain and Mountain Forest. In: Cambridge UK.
Vapnik, V.N., 1995. The Nature of Statistical Learning Theory. Springer, New York.
Vazquez-Amabile, G.G., Engel, B.A., 2005. Use of SWAT to compute groundwater table depth and streamflow in the Muscatatuck River watershed. Transactions of the Asae 48 (3), 991–1003.
Wang, A., Zeng, X., 2012. Evaluation of multireanalysis products with in situ observations over the Tibetan Plateau. J. Geophys. Res.-Atmos. 117. http://dx.doi.org/10.1029/2011jd016553.
Wang, X., Yang, T., Shao, Q., Acharya, K., Wang, W., Yu, Z., 2012. Statistical downscaling of extremes of precipitation and temperature and construction of their future scenarios in an elevated and cold zone. Stoch. Env. Res. Risk A. 26 (3), 405–418. http://dx.doi.org/10.1007/s00477-011-0535-z.
Wang, W., Xing, W., Shao, Q., Yu, Z., Peng, S., Yang, T., Yong, B., Taylor, J., Singh, V.P., 2013. Changes in reference evapotranspiration across the Tibetan Plateau: observations and future projections based on statistical downscaling. J. Geophys. Res.-Atmos. 118 (10), 4049–4068. http://dx.doi.org/10.1002/jgrd.50393.
Wang, X., Yang, T., Wortmann, M., Shi, P., Hattermann, F., Lobanova, A., et al., 2016. Analysis of multi-dimensional hydrological alterations under climate change for four major river basins in different climate zones. Clim. Chang. 141, 1–16.
Weedon, G.P., Gomes, S., Viterbo, P., Shuttleworth, W.J., Blyth, E., Oesterle, H., Adam, J.C., Bellouin, N., Boucher, O., Best, M., 2011. Creation of the WATCH forcing data and its use to assess global and regional reference crop evaporation over land during the twentieth century. J. Hydrometeorol. 12 (5), 823–848. http://dx.doi.org/10.1175/2011jhm1369.1.
Wetterhall, F., Halldin, S., Xu, C.Y., 2005. Statistical precipitation downscaling in central Sweden with the analogue method. Journal of Hydrology 306 (1–4), 174–190. http://dx.doi.org/10.1016/j,jhydrol.2004.09.008.
WMO-Mo.168, 2008. Guide to hydrological practices. In: Hydrology - From Measurement to Hydrological Information. WMO-Mo.168, Sixth edition. vol. 1.
Xu, J., Chen, Y., Ji, M., Lu, F., 2008. Climate change and its effects on runoff of Kaidu River, Xinjiang, China: a multiple time-scale analysis. Chin. Geogr. Sci. 18 (4), 331–339. http://dx.doi.org/10.1007/s11769-008-0331-y.
Xu, J., Chen, Y., Lu, F., Li, W., Zhang, L., Hong, Y., 2011. The Nonlinear trend of runoff and its response to climate change in the Aksu River, western China. Int. J. Climatol. 31 (5), 687–695. http://dx.doi.org/10.1002/joc.2110.
Yang, T., Hao, X., Shao, Q., Xu, C.-Y., Zhao, C., Chen, X., Wang, W., 2012. Multi-model ensemble projections in temperature and precipitation extremes of the Tibetan Plateau in the 21st century. Glob. Planet. Chang. 80-81, 1–13. http://dx.doi.org/10.1016/j.gloplacha.2011.08.006.
Yang, T., Wang, X., Yu, Z., Krysanova, V., Chen, X., Schwartz, F.W., Sudicky, E.A., 2014. Climate change and probabilistic scenario of streamflow extremes in an alpine region. J. Geophys. Res.-Atmos. 119 (14), 8535–8551. http://dx.doi.org/10.1002/2014jd021824.
Yang, T., Wang, C., Chen, Y., Chen, X., Yu, Z., 2015. Climate change and water storage variability over an arid endorheic region. J. Hydrol. 529, 330–339. http://dx.doi.org/10.1016/j.jhydrol.2015.07.051.
Yang, T., Cui, T., Xu, C.-Y., Ciais, P., Shi, P., 2017a. Development of a new IHA method for impact assessment of climate change on flow regime. Glob. Planet. Chang. 156, 68–79. http://dx.doi.org/10.1016/j.gloplacha.2017.07.006.
Yang, C., Wang, N., Wang, S., 2017b. A comparison of three predictor selection methods for statistical downscaling. Int. J. Climatol. 37 (3), 1238–1249. http://dx.doi.org/10.1002/joc.4772.
Zeng, X., Kundzewicz, Z.W., Zhou, J., Su, B., 2012. Discharge projection in the Yangtze River basin under different emission scenarios based on the artificial neural networks. Quat. Int. 282, 113–121. http://dx.doi.org/10.1016/j.quaint. 2011.06.009.
Zhang, Q., Xu, C.-Y., Chen, Y.D., Yang, T., 2009a. Spatial assessment of hydrologic alteration across the Pearl River Delta, China, and possible underlying causes. Hydrol. Process. 23 (11), 1565–1574. http://dx.doi.org/10.1002/hyp.7268.
Zhang, X., Liang, F., Srinivasan, R., Van Liew, M., 2009b. Estimating uncertainty of streamflow simulation using Bayesian neural networks. Water Resour. Res. 45. http://dx.doi.org/10.1029/2008wr007030.
Zhang, X., Liang, F., Yu, B., Zong, Z., 2011. Explicitly integrating parameter, input, and structure uncertainties into Bayesian Neural Networks for probabilistic hydrologic forecasting. J. Hydrol. 409 (3–4), 696–709. http://dx.doi.org/10.1016/j.jhydrol.2011.09.002.
Zhou, X., Yang, T., Shi, P., Yu, Z., Wang, X., Li, Z., 2017. Prospective scenarios of the saltwater intrusion in an estuary under climate change context using Bayesian neural networks. Stoch. Env. Res. Risk A. 31 (4), 981–991. http://dx.doi.org/10.1007/s00477-017-1399-7.
Zhuang, X.W., Li, Y.P., Nie, S., Fan, Y.R., Huang, G.H., 2018. Analyzing climate change impacts on water resources under uncertainty using an integrated simulation-optimization approach. J. Hydrol. 556, 523–538. http://dx.doi.org/10.1016/j.jhydrol.2017.11.016.